Conclusions

An explicit calculation procedure for the dynamic geometry of TV nozzles was presented. Relation of the geometry to the flow performances was elaborated and used to create a model for determining the flow coefficient and a maximum effective vectoring angle. This model was then compared with experimental data. The geometric predictions compared proved to be able to predict the upper bound of the effective vectoring angle very well, whereas the geometry only was proven to describe the variation in the flow coefficient with vectoring, but not the conventional flow coefficient.

Though the prediction decreased in precision with the addition of afterburning, it remains within experimental accuracy. As the flaps on the nozzle were shortened, the prediction diverged from the nozzle data as a function of vectoring angle, proving the dependence of jet performance on the nozzle divergence angle. In other words, the greater the divergence angle, the less ideal the jet expansion. Thus, the geometrical predictions have been verified for quasi-ideal cases and can be used in future TV nozzle design to reduce costly experimental investigations.

Further, it may be implemented to evaluate current TV nozzle performances to enhance aircraft and defense simulations, as well as provide realistic initial conditions for future numerical vertical/standard takeoff and landing/TV jet performance studies. In the future NPR influence on nozzle performance may be included in this procedure for a more robust nozzle performance prediction across the NPR range.

References

[1]Mace, J., Smereczniak, P., Krekeler, G., Bowers, D., MacLean, M., and Thayer, E., "Advanced Thrust Vectoring Nozzles for Supercruise Fighter Aircraft," AIAA Paper 89-2816, 1989.

[2]Burken, J., Burcham, F., Maine, T., Feather, J., Goldthorpe, S., and Kahler, J., "Flight Test of a Propulsion-Based Emergency Control System on the MD-11 Airplane with Emphasis on the Lateral Axis," NASA-TM-4746, July 1996.

[3]Gal-Or, B., "Complete Thrust Vectoring Flight Control for Future Civil Jets, F-22 Superiority Fighter and Cruise Missiles. Part I: Vectored F-22, F-16 and F-15," *International Journal of Turbo and Jet Engines*, 10, 1993, pp. 1–17.

[4]Gal-Or, B., "Fundamental Concepts of Vectored Propulsion," *Journal of Propulsion and Power*, Vol. 6, No. 6, 1990, p. 747.

[5]Gal-Or, B., *Vectored Propulsion Supermaneuverability and Robot Aircraft*, Berlin, Springer-Verlag, 1991, pp. 1–294.

[6]Wilson, E., "A Two-Spool Turbofan Thrust Vectoring Analysis," M.Sc. Thesis, Technion—Israel Inst. of Technology, Haifa, Israel, Faculty of Mech. Engineering, July 1997.

[7]Matesanz, A., Velaquez, A., and Rodriguez, M., "Aerodynamic Prediction of Thrust-Vectoring Nozzles," *Journal of Propulsion and Power*, Vol. 14, No. 2, 1998, pp. 241–246.

[8]Carlson, John R., "A Nozzle Internal Performance Prediction Method," NASA-TP-3211, Oct. 1992.

[9]Matesanz, A., and Velaquez, A., "Performance Analysis of an Axisymmetric Thrust Vectoring Nozzle Using the FUNSIF3D Code," AIAA Paper 95-2743, June 1995.

[10]Decher, R., "Mass Flow and Thrust Performance of Nozzles with Mixed and Unmixed Nonuniform Flow," *Journal of Fluids Engineering*, 117, Dec. 1995, pp. 617–622.

[11]Persen, L. N., Oiann, H., and Mazumdar, H. P., "The Round Thermal Jet: Undisturbed and in a Crossflow," *International Journal Heat and Mass Transfer*, Vol. 36, No. 6, 1993, pp. 1598, 1599.

[12]Elangovan, S., Solaiappan, A., and Rathakrishnan, E., "Studies on Twin Elliptic Jets," *Aeronautical Journal*, Vol. 100, No. 997, 1996, pp. 295, 296.

[13]Wilson, E., Adler, D., Gal-Or, B., Sherbaum, V., and Lichtsinder, M., "Optimizing Subcritical-Flow Thrust-Vectoring of Converging-Diverging Nozzles," *Journal of Propulsion and Power*, Vol. 16, No. 2, 2000, pp. 202–206.

[14]Berrier, B. L., and Re, R. J., "Investigation of Convergent-Divergent Nozzles Applicable to Reduced-Power Supersonic Aircraft," NASA-TP-1766, 1980.

[15]Carson, G. T., and Capone, F. J., "Static Internal Performance of an Axisymmetric Nozzle with Multiaxis Thrust-Vectoring Capability," NASA-TM-4237, Feb. 1991.

Combustion Characteristics of Ethylene in Scramjet Engines

A. A. Taha,* S. N. Tiwari,† and T. O. Mohieldin‡
Old Dominion University, Norfolk, Virginia 23529

Introduction

MOST of the scramjet combustion studies, currently being conducted, use liquid hydrocarbon fuels or hydrogen. The use of hydrocarbon fuels in volume-limited systems will require an ignitor and some form of combustion enhancement.[1] The results of the early tests conducted by Kay et al.[2,3] clearly demonstrated that the supersonic combustion of various hydrocarbon fuels could be achieved; although for many test conditions special externally mounted piloting devices were required to initiate and stabilize the flame.

The piloted-supersonic combustion experiments strongly recommended that hydrogen piloting is highly effective for a variety of fuels including methane and kerosene. A monopropellent, OTTO fuel, was successfully used as an effective pilot in the scramjets.[1] Other results showed that silane/hydrogen mixtures were effective pilots for ethylene and kerosene combustion.[4]

Ethylene C_2H_4 is a primary fuel itself and is also produced in large amounts during the combustion of methane CH_4, ethane C_2H_6, and other higher hydrocarbons.[5] Ethylene is often chosen for the hydrocarbon-fueled scramjet engines tests because it is used as a surrogate test fuel for hydrocarbon fuels.

The intent of this study is to investigate the supersonic combustion flowfield of ethylene as a candidate hydrocarbon fuel in scramjet engines. Special attention is paid to studying the effect of piloting on the main flame initialization and stabilization. During this phase of the study, piloting with gaseous ethylene was used while the proposed objective is to use hydrogen as a pilot fuel. Because of the unavailability of experimental data for the supersonic combustion of ethylene, the verification of the present numerical results with existing experimental results could not be achieved. Therefore, the validation of the computational fluid dynamics (CFD) Fluent code[6] was achieved by comparing cold-flow numerical results with the pertinent experimental results of McDaniel et al.[7] This verification study was published in Ref. 8

Theoretical Model and Computational Procedure

The schematic diagram for the configuration used in the present study is presented in Fig. 1 in which a rearward-facing step is located at the upper longitudinal wall. Sonic pilot ethylene is injected parallel to the incoming airstream via three 1-mm circular holes that are equally distributed at the base of the step. The pilot ethylene static temperature is 500 K with equivalence ratio of 0.06 calculated based on the mass flow rate of the incoming supersonic air inlet. The inflow is vitiated air with Mach number = 1.756 to simulate the enthalpy level of the typical conditions at the combustor inlet. The total temperature is 1800 K while the total pressure is set to be 431.762 kPa. The vitiated supersonic air inlet contains H_2O with mass fraction of 0.17. A 15-deg wedge is located downstream of the step and upstream of the main normal injection. The combination

Received 5 January 2001; revision received 10 September 2001; accepted for publication 10 December 2001.

*Graduate Research Assistant, Department of Mechanical Engineering, College of Engineering and Technology. Student Member AIAA.

†Eminent Professor/Scholar, Department of Mechanical Engineering, College of Engineering and Technology. Associate Fellow AIAA.

‡Professor, Mechanical Engineering Technology Department, College of Engineering and Technology.

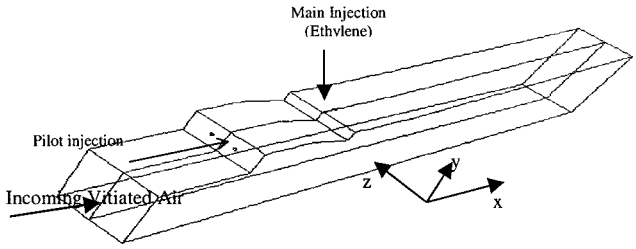

Fig. 1 Schematic diagram for the case study.

of the rearward-facing step and the wedge forms a cavity-like configuration that helps in enhancing the fuel-air mixing in addition to initiate and stabilize the main flame.

The configuration used in this study uses the symmetry condition at the midspan location; therefore, just one-half of the physical domain is simulated to minimize the computational time.

While using the same basic configuration and inlets boundary conditions as of Owens et al.,[9] slight differences in the dimensions are applied. The step height H is 10 mm. Gaseous ethylene, as the main fuel, is injected at four step heights downstream of the step with a sonic speed normal to a supersonic airstream. The main injection static temperature is 300 K with equivalence ratio of 0.6 calculated based on the mass flow rate of the incoming supersonic air at inlet.

An unstructured grid with 180,360 cells is used for accurate meshing of the circular cross-section injection holes. The normal injection evolves the three-dimensional nature of the physical problem. Accordingly, the three-dimensional version of the CFD code is used in the simulation.

The CFD code used in this study is the Fluent commercial code (version 5).[6] The code is a finite volume-based CFD code, which solves steady and unsteady three-dimensional Reynolds-averaged Navier–Stokes equations. The renormalization-group κ–ϵ turbulence model is used in the present study.

At the supersonic inflow boundaries the total and static pressures, the total temperature, and the species mass fractions are specified. For these supersonic inflow boundaries uniform conditions were assumed for the primitive parameters. At the supersonic outflow boundaries first-order extrapolation for all parameters is used. All walls and step boundaries are treated as no-slip adiabatic surfaces.

The initial conditions were set by applying freestream inlet conditions throughout the entire flowfield. The solution convergence is judged by reaching a scaled residual value of at most 10^{-3} for every calculated parameter. The most important flowfield parameters such as temperature, pressure, velocity magnitude, and CO_2 mass fraction are averaged over all grid cells at different crossflow planes along the combustor length using the mass-weighted approach. At the convergence condition these averages should show unchangeable values with the solution iterations as additional way to check for the solution convergence.

Results and Discussion

Figure 2 shows the distribution of the average static pressure and temperature at the upper wall along the combustor length. Fourteen crossflow lines marking the intersection of the combustor upper wall and the corresponding crossflow planes are defined along the upper wall length. The points on the two curves of Fig. 2 represent the arithmetic averages of static pressure and temperature respectively at the centers of all grid cells of the 14 intersection lines. The typical upper-wall average static-pressure distribution is presented by the solid line in Fig. 2. Because of the expansion waves formed around the step edge, the static pressure decreases, reaching its minimum value just upstream of the wedge body. The oblique shock wave formed by the wedge body increases the pressure. The maximum pressure location is coincided with the main normal injection station. The high normal injection pressure creates a low-pressure region near upstream of the injection area. This forms a recirculation region that entrains the incoming supersonic air to be mixed with the fuel and forming a combustible mixture supporting the main flame.

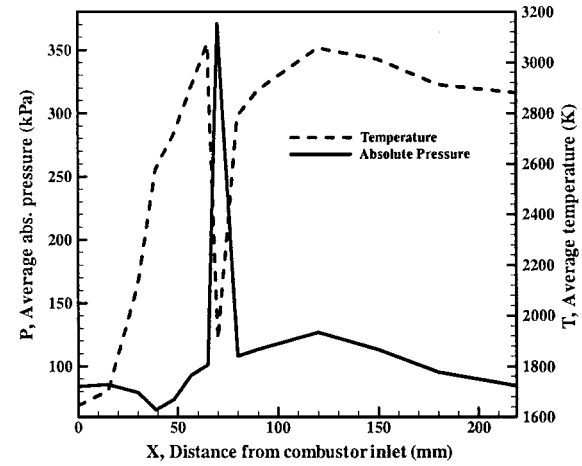

Fig. 2 Average wall static pressure and temperature distribution along the combustor length.

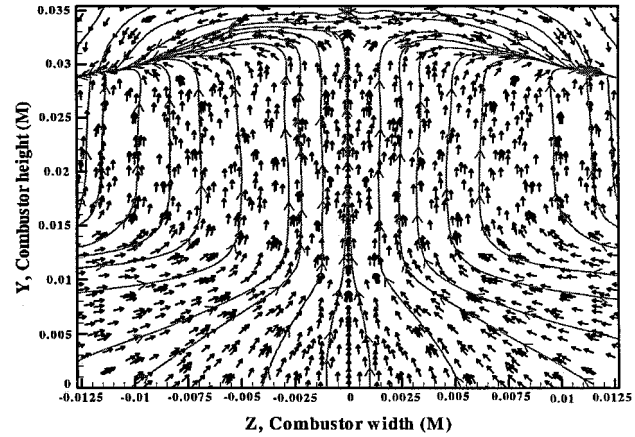

Fig. 3 Velocity vectors at x = 40 mm cross plane.

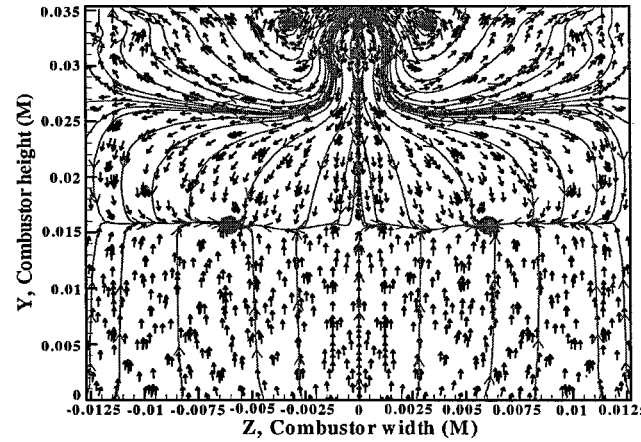

Fig. 4 Velocity vectors at x = 70 mm cross plane.

Because of the shock reflection off the lower wall, the upper-wall static pressure increases followed by a continuous pressure decrease caused by the 3-deg combustor divergence.

The upper-wall average temperature distribution is presented by the dotted line in Fig. 2. The frictional heating at the upper-wall surface increases the surface temperature downstream of the combustor inlet. The effect of the pilot flame can be shown by noting the location of the first peak in the temperature plot. This first peak coincides with the pilot flame tip at the wedge edge that forms a

high-temperature region near upstream of the main normal injection location. This region forms a continuous high-temperature area, the effect of which resembles that of a sparkplug in helping initializing and holding the main flame. Igniting the main fuel injected leads to the second increase of the upper-wall temperature, reaching its peak downstream of the injection station. The flow expansion caused by the 3-deg combustor divergence reduces the temperature towards the combustor exit. Other results for this case study are presented in Ref. 10.

The flowfield features are presented in Figs. 3 and 4. The velocity vectors plot with the superimposed streamlines are depicted at two crossflow locations. Figure 3 shows the vectors in the cavity region downstream of the pilot injection at $X = 40$ mm. The vectors at the main injection location, $X = 70$ mm, are shown in Fig. 4. The two plots exhibit the interaction between the incoming supersonic airflow and the pilot and main ethylene injections. The recirculations formed in the cavity are caused by the expansion effect of the step. The parallel pilot injections intensify the recirculations pattern in the cavity. This can be observed in Fig. 3 at the pilot injection location, $Y = 30.5$ mm. Figure 4 shows the interaction between the incoming supersonic airflow and the vortices formed as a result of the normal injection. This effect is manifested by observing the two counterflows at the midcombustor span, $Y \sim 15$ mm. The confrontation of the two counterflows is presented by the two loops in the streamlines around $Z = \pm 0.0065$ m. The counterflow has the effect of increasing the diffusion between the fuel and air and eventually enhancing the fuel/air mixing. The vortices formed around the fuel injection areas help in promoting the air-fuel mixing process and consequently lead to more efficient combustion.

Conclusions

The step plays a remarkable role in enhancing the fuel/air mixing. The pilot flame stabilizes and supports the main flame formed by the main vertical injection. The existence of the wedge downstream of the rearward-facing step helps in initiating and stabilizing the main flame. Work is underway to analyze the effect of the gaseous hydrogen pilot injection on the combustion of the sonic normal ethylene flow.

Acknowledgments

This work was supported, in part, by the Old Dominion University's Institute for Scientific and Educational Technology through NASA Langely Research Center, Cooperative Agreement NCC1-349. The cooperative agreement was monitored by Samuel E. Massenberg, Director, Office of Education.

References

[1]Northam, G. B., "Workshop Report: Combustion in Supersonic Flow," *21st JANNAF Combustion Meeting*, Oct. 1984.

[2]Kay, I. W., Chiappetta, L., and McVey, J. B., "Hydrocarbon-Fueled Scramjet, Combustor Investigation," Technical Rept. AFAPL-TR-68-146, Vol. IV, May 1969.

[3]Kay, I. W., McVey, J. B., Kepler, C. E., and Chiappetta, L., "Hydrocarbon-Fueled Scramjet, Piloting and Flame Propagation Investigation, Combustor Investigation," Technical Rept. AFAPL-TR-68-146, Vol. IX, May 1971.

[4]Northam, G. B., and Anderson, G. Y., "Supersonic Combustion Ramjet Research at Langley," AIAA Paper 86-0159, Jan. 1986.

[5]Westbrook, C. K., and Dryer, F. L., "Chemical Kinetics Modeling of Hydrocarbon Combustion," *Progress in Energy and Combustion Science*, Vol. 10, 1984, pp. 1–57.

[6]*Fluent Version 5.0 User's Guide*, Fluent, Inc., Lebanon, New Hampshire, 1998.

[7]McDaniel, J., Fletcher, D., Hartfield, R., and Hollo, S., "Staged Transverse Injection into Mach 2 Flow Behind a Rearward-Facing Step: A 3-D Compressible Test Case for Hypersonic Combustor Code Validation," AIAA Paper 91-5071, Dec. 1991.

[8]Taha, A. A., Tiwari, S. N., and Mohieldin, T. O., "Validation of Fluent CFD Code in Supersonic Flow Fields," AIAA Paper 2001-2637, June 2001.

[9]Owens, M., Segal, C., and Auslender, A. H., "Effects of Mixing Schemes on Kerosene Combustion in a Supersonic Air Stream," *Journal of Propulsion and Power*, Vol. 13, No. 4, 1997, pp. 525–531.

[10]Taha, A. A., Tiwari, S. N., and Mohieldin, T. O., "Numerical Simulation of Ignition/Combustion Characteristics of Ethylene in Supersonic Air Streams," AIAA Paper 2000-3584, July 2000.

High-Intensity Sound Absorption at an Orifice with Bias Flow

Xiaodong Jing* and Xiaofeng Sun†
Beijing University of Aeronautics and Astronautics, Beijing 100083, People's Republic of China

I. Introduction

A PERFORATED liner has been widely used to control noise or suppress combustion instability in the afterburner of a jet engine or the combustor of a rocket engine. For the suppression of combustion instability, cooling air is introduced through the orifices to protect the liner from being burnt. Previous research[1] showed that mean bias flow also enhances the sound absorption at an orifice. It was further proposed that bias flow could be employed to control the liner impedance, thereby greatly increasing the duct attenuation.[2] Various models[3,4] have been set up to study the bias flow effect on the orifice impedance. A common feature of the preceding models is that the incident sound is assumed to be of low intensity and to interact linearly with mean bias flow. On the other hand, considerable research[1,4–7] has been carried out on the nonlinear sound dissipation at an orifice in the absence of mean flow, and it was shown that the velocity of the sound-excited oscillatory flow in the orifice could be very large at high sound pressure levels. Thus, in the situation of high-intensity sound incident on an orifice with bias flow, there will be little evidence for assuming linear flow–acoustic interaction. To the authors' knowledge, there has been experimental investigations[8] on the combining effect of mean bias flow and high sound intensity on the orifice impedance, but the related theoretical studies are very few.

Previous studies have provided persuasive evidence that the sound absorption that occurs at an orifice is due to the conversion of the acoustic energy into vortical energy, either in the presence of mean bias flow[3] or at high sound intensity.[4–7] It is reasonable to believe that this mechanism is also applied to the high-intensity sound absorption at an orifice in the presence of bias flow. From this point of view, we first employ a discrete vortex model to simulate the vortex shedding process produced by high-intensity sound at an orifice with bias flow. This model is also used to obtain some quantitative results, including the average velocity through the orifice and the orifice acoustic impedance. In addition, a quasi-steady model is further developed to study this phenomenon.

II. Theoretical Models

Consider the phenomenon that a low-frequency, high-amplitude sinusoidal sound is incident on a circular orifice of radius R that is located in an infinitely thin, rigid plate. There is also mean bias flow through the orifice. The total pressure difference Δp across the orifice plate can be written as follows:

$$\Delta p = P_B + P_A \cos(\omega t) \tag{1}$$

where P_B is steady pressure difference producing bias flow, P_A is the amplitude of the incident sound, ω is angular frequency, and t is time.

A. Discrete Vortex Model

The discrete vortex model of Ref. 6 is modified to study the sound-excited vortex shedding at the orifice. To obtain a smooth

Received 16 March 2001; revision received 20 October 2001; accepted for publication 20 November 2001.

*Associate Professor, Department of Jet Propulsion.
†Professor, Department of Jet Propulsion. AIAA Member.